Chinese Physics Letters

EXPRESS LETTER

On the Precise Boundary of the Néel Antiferromagnetic Phase in the Shastry-Sutherland Model

Cite as: Rongyi Lv *et al*. 2026 *Chin. Phys. Lett.* **43** 120705

Recommended Articles

Deconfined Quantum Critical Point: A Review of Progress
Yi Cui, Rong Yu, and Weiqiang Yu
Chin. Phys. Lett. **42**, 047503 (2025)

Observation of Topological Hall Effect and Nernst Effect in the Canted Antiferromagnetic Phase of $MnBi_2Te_4$
Haiyang Yang *et al*.
Chin. Phys. Lett. **42**, 080706 (2025)

Probing the Néel Order in Altermagnetic RuO_2 Films via X-Ray Magnetic Linear Dichroism
Yi-Chi Zhang *et al*.
Chin. Phys. Lett. **42**, 027301 (2025)

Quantum Spin Liquid Phase in the Shastry–Sutherland Model Detected by an Improved Level Spectroscopic Method
Ling Wang, Yalei Zhang, and Anders W. Sandvik
Chin. Phys. Lett. **39**, 077502 (2022)

Augmenting Density Matrix Renormalization Group with Matchgates and Clifford Circuits
Jiale Huang, Xiangjian Qian, Zhendong Li, and Mingpu Qin
Chin. Phys. Lett. **43**, 040708 (2026)

A series journal of Chinese Physical Society distributed by IOP Publishing

Chinese Physics Letters

Chin. Phys. Lett. **43** 120705 (2026)

EXPRESS LETTER

DOI: 10.1088/0256-307X/43/12/120705
CSTR: 32039.14.0256-307X.43.12.120705

On the Precise Boundary of the Néel Antiferromagnetic Phase in the Shastry-Sutherland Model

Rongyi Lv(吕融一)[1], Xiangjian Qian(钱湘坚)[1,2], and Mingpu Qin(秦明普)[1,3,*]

[1]Key Laboratory of Artificial Structures and Quantum Control (Ministry of Education), School of Physics and Astronomy, Shanghai Jiao Tong University, Shanghai 200240, China
[2]Tsung-Dao Lee Institute, Shanghai Jiao Tong University, Shanghai 200240, China
[3]Hefei National Laboratory, Hefei 230088, China

[*]Corresponding author. Email: qinmingpu@sjtu.edu.cn

The ground state phase diagram of the Shastry-Sutherland model remains controversial. In particular, the nature of the transition between the plaquette valence bond solid (PVBS) phase and the Néel antiferromagnetic (AFM) phase is still under debate. While some studies suggest a direct transition between the two phases, others propose the existence of a narrow intermediate quantum spin liquid regime. To address this issue, we perform large-scale Density Matrix Renormalization Group calculations to determine the Néel AFM phase boundary in the Shastry-Sutherland model. By applying staggered boundary pinning fields and directly measuring the bulk staggered magnetization, and through systematic extrapolations with respect to truncation error as well as careful finite-size scaling, we find that the staggered magnetization remains finite across the controversial region $0.78 \lesssim J_1/J_2 \lesssim 0.81$, which was suggested to host a quantum spin liquid phase in some studies. Together with the previously established consensus placing the PVBS phase boundary at $J_1/J_2 \approx 0.78$, these results, within the resolution of the present calculations, provide evidence against the existence of an intermediate quantum spin liquid phase and support a direct PVBS–Néel AFM transition in the Shastry-Sutherland model.

Introduction

Frustrated quantum magnets provide a fertile platform for exploring exotic quantum phases and phase transitions beyond the conventional Landau-Ginzburg paradigm. Strong frustration and quantum fluctuations may give rise to long-range entangled states such as quantum spin liquids (QSLs) [1–5], which lack long-range order even at zero temperature and fall outside the traditional symmetry-breaking framework. Elucidating the nature of such exotic phases is of fundamental importance for the study of strongly correlated quantum magnets.

Among various frustrated quantum magnet models, the Shastry-Sutherland model [6] has attracted significant attention over the past few decades. It is also believed to capture the essential physics of the quasi-two-dimensional material $SrCu_2(BO_3)_2$ [7–15]. The Hamiltonian of the Shastry-Sutherland model is given by

$$H = J_1 \sum_{\langle i,j \rangle} \boldsymbol{S}_i \cdot \boldsymbol{S}_j + J_2 \sum_{\langle\langle i,j \rangle\rangle} \boldsymbol{S}_i \cdot \boldsymbol{S}_j, \tag{1}$$

where $\boldsymbol{S}_i$ is the spin-1/2 operator at site i. The antiferromagnetic coupling constants J_1 and J_2 represent the nearest-neighbor ($\langle i,j \rangle$) and next-nearest-neighbor ($\langle\langle i,j \rangle\rangle$) interactions, respectively. As shown in Fig. 1(a), the nearest-neighbor bonds are represented as black pairs and the next-nearest-neighbor bonds are represented as blue pairs. Different from the J_1–J_2 Heisenberg model on the square lattice, the Shastry-Sutherland model contains only part of the next-nearest-neighbor interactions. But same as in the J_1–J_2 Heisenberg model, the competition between J_1 and J_2 couplings in the Shastry-Sutherland model induces strong frustration, resulting in a diverse and complex ground state phase diagram. It is widely accepted that for $J_1/J_2 \lesssim 0.68$, the system resides in a dimer singlet phase, while for $J_1/J_2 \gtrsim 0.82$, it enters the Néel antiferromagnetic (AFM) phase [8,16–28]. Between these two phases, an intermediate plaquette valence bond solid (PVBS) phase in the range of $0.68 \lesssim J_1/J_2 \lesssim 0.78$ has been established in previous studies [8,16–28].

However, the nature of the phase transition between the PVBS and AFM phases remains under active debate. On the one hand, several numerical studies suggest a direct transition between the two ordered phases. Early density matrix renormalization group (DMRG) results proposed a deconfined quantum critical point (DQCP) with emergent O(4) symmetry at $J_1/J_2 = 0.77$ [17], while recent finite projected entangled pair state (PEPS) calculations also support a DQCP scenario, but locating the transition at $J_1/J_2 = 0.828$ [22]. Alternatively, studies based on projected entangled simplex state [21] and DMRG [25] support a weakly first-order transition at $J_1/J_2 \approx 0.79$. On the other hand, multiple numerical investigations, including functional renormalization group [18], DMRG [19], neural quantum states [24], and very recent infinite PEPS (iPEPS) [28], have suggested the existence of a narrow intermediate QSL phase in the range of $0.78 \lesssim J_1/J_2 \lesssim 0.82$. Despite these different scenarios, previous studies have established a broad consensus that the PVBS phase terminates at $J_1/J_2 \approx 0.78$ [17–21,23–25,28]. Therefore, the key unresolved question is whether Néel AFM order develops at the boundary of the PVBS phase, corresponding to a direct PVBS–Néel AFM transition, or only at a larger value of J_1/J_2, leaving an intervening magnetically disordered region that may host a QSL phase.

A central difficulty in resolving this issue lies in the reliable determination of the AFM order parameter near the phase boundary. In finite-size simulations, preserving $SU(2)$ spin symmetry precludes a direct measurement of the staggered magnetization m_s from the local spin expectation values. Approaches based on finite-size scaling of spin correlations effectively compute m_s^2 rather than m_s itself and can therefore suffer from significant uncertainties when the magnetic order parameter is very small [25,29–31], especially in the narrow parameter region where different phases may compete. In such cases, distinguishing a genuinely disordered phase from a weakly ordered AFM phase is challenging.

In this work, we revisit this problem using large-scale DMRG [32–34] simulations on cylindrical geometries. To more reliably detect the possible weak AFM order, we apply staggered pinning fields

Received 7 October 2026; accepted 30 October 2026; published 11 November 2026
© 2026 Chinese Physical Society and IOP Publishing Ltd. All rights, including for text and data mining, AI training, and similar technologies, are reserved.

Check for updates

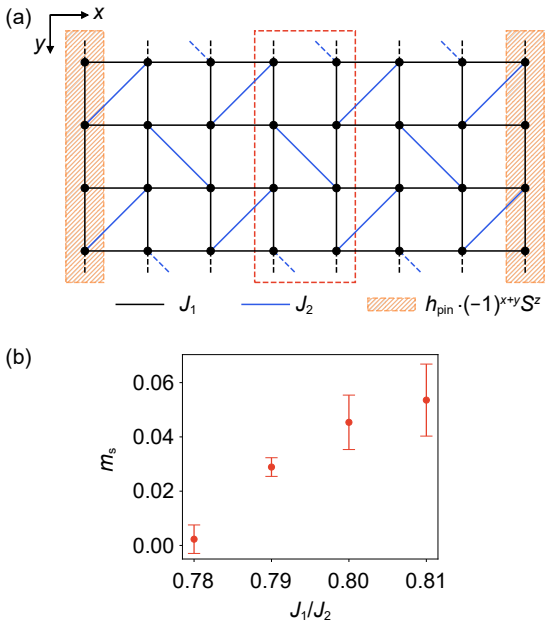

Fig. 1. Shastry-Sutherland model and the results for staggered magnetization. (a) Shastry-Sutherland model on a 4×8 cylinder with open boundary conditions in the x direction and periodic boundary conditions in the y direction. The black and blue lines represent the J_1 and J_2 interactions, respectively. We set $J_2 = 1$ throughout this work. A pinning field along the z direction with strength h_{pin} is applied at the open boundaries (orange hatched regions). The staggered magnetization m_s is measured on the two central columns (red dashed box). (b) Staggered magnetization m_s as a function of J_1/J_2, measured with a pinning field ($h_{pin} = 0.5$) and extrapolated to the thermodynamic limit using results from multiple cylinders with different aspect ratios (details in Figs. 2 and 4). The extrapolated m_s indicates that the lower boundary of the Néel AFM phase lies near $J_1/J_2 \approx 0.78$.

at the open boundaries of the cylinders [35]. By explicitly breaking the $SU(2)$ symmetry, we can directly probe the bulk staggered magnetization. For each finite geometry, we perform controlled extrapolations with truncation error, followed by finite-size scaling to the thermodynamic limit. Following Ref. [35], we compare the finite-size scaling of the results with different aspect ratios and determine the staggered magnetization in the thermodynamic limit as the converged value. Our results demonstrate that the staggered magnetization remains finite throughout the previously disputed region $0.78 \lesssim J_1/J_2 \lesssim 0.81$. These findings, together with the previously established consensus placing the PVBS phase boundary at $J_1/J_2 \approx 0.78$ [17–21,23–25,28], provide evidence against the existence of an intermediate QSL phase and support a direct transition between the PVBS and Néel AFM phases in the Shastry-Sutherland model within the resolution of the present calculations.

Method

DMRG has established itself as arguably the most powerful numerical method for studying one-dimensional and quasi-one-dimensional quantum many-body systems. Its efficiency originates from the underlying matrix product state (MPS) variational ansatz [36], which provides a compact representation of area-law entangled states for one-dimensional systems [34,37–39], thereby capturing the essential entanglement structure of the system at a relatively low computational cost. In DMRG, the bond dimension D governs the maximum entanglement that can be captured by the state, directly determining the numerical precision of the DMRG results. DMRG can also accurately solve the ground state of spin models on two-dimensional cylinders with width around 10 by pushing the bond dimension to very large values [40–44]. In this work, we exploit the $U(1)$ symmetry associated with total S^z conservation and push the bond dimension up to as

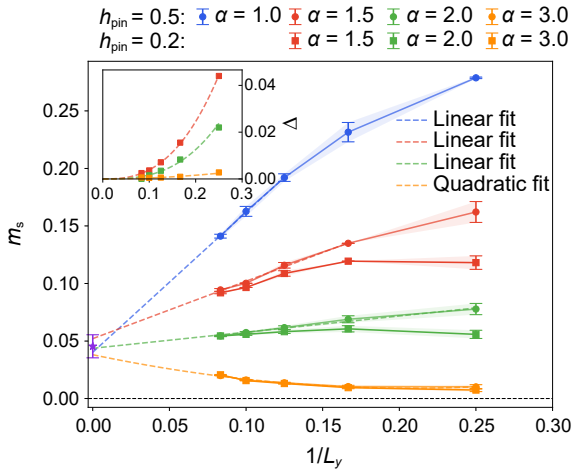

Fig. 2. Finite-size scaling of the staggered magnetization m_s at $J_1/J_2 = 0.8$ with two pinning field strengths, $h_{pin} = 0.5$ and 0.2. Values extrapolated to zero DMRG truncation error are shown (see Figs. S3–S5 in the Supplementary Materials (SM) [45] for the corresponding extrapolations). Data for systems with different aspect ratios α are extrapolated to the thermodynamic limit ($1/L_y \to 0$). Inset: The difference in m_s between the two pinning fields, denoted as Δ, as a function of $1/L_y$. We can see Δ vanishes as $1/L_y \to 0$, demonstrating that the extrapolated staggered magnetization is independent of the pinning field strength. The converged finite extrapolated value of m_s for systems with different aspect ratios indicates long-range Néel AFM order at this coupling ratio.

large as $D = 30000$ for the widest systems ($L_y = 12$), enabling us to suppress the truncation error to the order of 10^{-6} and perform reliable extrapolations for each finite-size system.

Figure 1(a) illustrates the Shastry-Sutherland model studied in this work on cylinders, where we impose open boundary conditions (OBC) in the x direction and periodic boundary conditions (PBC) in the y direction. Throughout this work, we set $J_2 = 1$ and express all energies and pinning field strengths in units of J_2. We define the aspect ratio $\alpha = L_x/L_y$, where L_x denotes the total number of columns along the x direction, including the two boundary columns on which the pinning fields are applied. To systematically approach the thermodynamic limit while mitigating finite-size effects, we mainly perform calculations on cylinders with aspect ratios $\alpha \in \{1.5, 2, 3\}$, with the cylinder width L_y reaching up to 12, and check the convergence of the results with different aspect ratios [30,35,43]. At the representative point $J_1/J_2 = 0.8$, we also study the square-like geometry with $\alpha = 1$ as an additional check of geometry-dependent finite-size effects.

To probe the magnetic order of the system, we follow the strategy in Ref. [35]. We apply staggered pinning fields along the z direction with strength h_{pin} at the open boundaries to explicitly break the $SU(2)$ symmetry. We primarily set $h_{pin} = 0.5$ in this work. At $J_1/J_2 = 0.8$, the staggered magnetizations obtained with $h_{pin} = 0.2$ and 0.5 agree in the thermodynamic limit (see Fig. 2 and its inset), indicating our conclusion is independent of the strength of the pinning fields. The application of boundary pinning fields enables a direct measurement of the staggered magnetization m_s in the bulk. Specifically, we define m_s as

$$m_s = \frac{1}{N_c} \sum_{i \in \text{central}} \eta_i \langle S_i^z \rangle, \tag{2}$$

where $\eta_i = \pm 1$ denotes the phase factor of the expected staggered pattern, and N_c is the number of sites included in the average. The summation is taken over the central region of the cylinder to reduce boundary-induced artifacts: for cylinders with even length L_x, we consider the two central columns, as illustrated by the red dashed box in Fig. 1(a), whereas for cylinders with odd L_x, we consider only the single central column. For cylinders with even length, the onsite staggered magnetizations in the central region generally take different values on the two sublattices, denoted as A and B, which are associated

with the two orthogonal orientations of the dimer bonds in the Shastry-Sutherland lattice. However, they should converge to the same value in the thermodynamic limit.

To account for this finite-size sublattice splitting, we perform independent linear extrapolations of the staggered magnetizations averaged separately over the A and B sites within the central region, denoted as m_s^A and m_s^B, as functions of the truncation error ε for each geometry. The extrapolated values in the $\varepsilon \to 0$ limit are subsequently averaged to yield the staggered magnetization for each finite geometry,

$$m_s = \frac{m_s^A + m_s^B}{2}. \tag{3}$$

The difference between m_s^A and m_s^B provides a measure of the finite-size splitting associated with the two inequivalent sublattices and is reflected in the error bars of the subsequent finite-size scaling analysis. The truncation-error extrapolations are shown in the SM [45]. Finally, the resulting values of m_s are extrapolated as a function of the inverse cylinder width $1/L_y$, to obtain the staggered magnetization in the thermodynamic limit.

Results

We first investigate systems with $J_1/J_2 = 0.8$, a representative point deep inside the intermediate QSL regime proposed in several previous studies [18,19,24,28]. To systematically approach the thermodynamic limit while mitigating finite-size effects, we perform DMRG simulations on cylinders with four distinct aspect ratios: $\alpha \in \{1, 1.5, 2, 3\}$. As shown in Fig. 2, the staggered magnetization exhibits different finite-size effects as expected [30,35]. For aspect ratios $\alpha = 1$ and 1.5, m_s decreases with the increase of the system size, while systems with aspect ratio $\alpha = 3$ show opposite behavior. Mild finite-size effects are found for aspect ratio $\alpha = 2$. A simple finite-size scaling of the staggered magnetization m_s with a boundary pinning field $h_{pin} = 0.5$ yields a consistent nonzero extrapolated value across all four geometries, with $m_s = 0.045(10)$ in the thermodynamic limit. The quoted uncertainty is chosen conservatively to encompass the spread among different aspect ratios, thereby accounting for geometry-dependent effects. These results indicate that $J_1/J_2 = 0.8$ lies in the Néel AFM phase.

We also check the effect of the strength of the pinning fields on the extrapolated staggered magnetization. As shown in the inset of Fig. 2, the difference of the values of staggered magnetization for $h_{pin} = 0.2$ and $h_{pin} = 0.5$ vanishes in the thermodynamic limit.

We also calculate the ground state energy density e at $J_1/J_2 = 0.8$. To reduce boundary effects, we calculate local site energies from the corresponding bond energies and average them over the two central columns for even L_x and the three central columns for odd L_x. For each finite geometry, the resulting average energy e is extrapolated to zero DMRG truncation error, with details in the SM [45]. The finite-size energies for $L_y = 6, 8, 10$, and 12 are then extrapolated using the power-law form $e(L_y) = e_\infty + AL_y^{-4}$, with the exponent 4 chosen to maximize the coefficient of determination R^2 among the tested fits. As shown in Fig. 3, the extrapolations for $h_{pin} = 0.2$ and 0.5 across multiple aspect ratios yield mutually consistent estimates, giving $e_\infty = -0.4490(1)$, in agreement with the recent iPEPS result $e_\infty = -0.44896(2)$ [28] and $e_\infty = -0.4490$ in Ref. [46]. We notice that despite the close agreement in ground state energy, different iPEPS-based calculations reach different conclusions regarding magnetic order. In Ref. [28], the authors find that the squared local magnetic moment extrapolates to zero through finite correlation length scaling, whereas the iPEPS study employing a single-layer framework [46] reports a finite extrapolated magnetization at this coupling. This discrepancy may arise from the sensitivity of the extrapolation near the critical region to the choice of scaling ansatz and fitting range.

After establishing that $J_1/J_2 = 0.8$ lies in the Néel AFM phase, we scan the interval $0.78 \le J_1/J_2 \le 0.81$ to determine the Néel AFM phase boundary on the small J_1/J_2 side. For these calculations, we

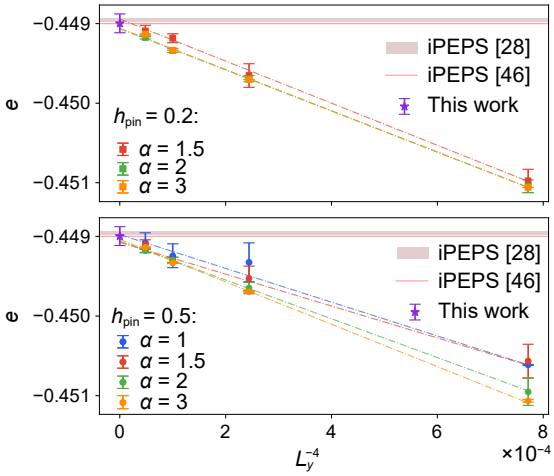

Fig. 3. Finite-size scaling of the ground state energy density e for the Shastry-Sutherland model at $J_1/J_2 = 0.8$. The bulk energies extrapolated to zero DMRG truncation error (see the SM [45] for details) for $L_y = 6, 8, 10$, and 12 with different aspect ratios α are shown. The upper and lower panels correspond to $h_{pin} = 0.2$ and 0.5, respectively. The resulting thermodynamic limit estimate, $e_\infty = -0.4490(1)$ (the purple star), is consistent with the previous iPEPS result [28,46].

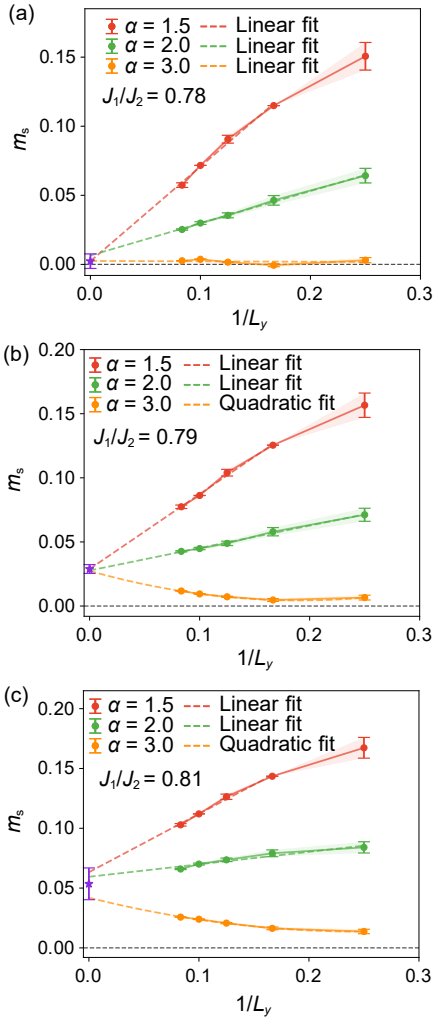

Fig. 4. Finite-size scaling of the staggered magnetization m_s extrapolated to zero DMRG truncation error (see the SM [45] for details) for different coupling ratios: (a) $J_1/J_2 = 0.78$, (b) 0.79, and (c) 0.81. All data are obtained with a pinning field strength of $h_{pin} = 0.5$. As in Fig. 2, m_s converges to the same value in the thermodynamic limit for systems with different aspect ratios α.

use the same pinning field strength of $h_{\text{pin}} = 0.5$. The systematic finite-size scaling for the specific values of $J_1/J_2 = 0.78, 0.79$, and 0.81 are presented in Fig. 4, showing the convergence of the staggered magnetization across multiple aspect ratios. The resulting extrapolated values of m_s are summarized as a function of the coupling ratio J_1/J_2 in the magnetic phase diagram shown in Fig. 1(b). As captured in this phase diagram, m_s exhibits a monotonic increase across the investigated interval.

At the lower bound of our investigated range, $J_1/J_2 = 0.78$, we obtain an extrapolated magnetization of $m_s = 0.0023(53)$, which is consistent with zero within uncertainty. In contrast, a finite extrapolated staggered magnetization is obtained at $J_1/J_2 = 0.79$. These results indicate that the lower boundary of the Néel AFM phase lies near $J_1/J_2 \approx 0.78$, with a coupling ratio resolution of approximately 0.01. We notice that at $J_1/J_2 = 0.78$ for the 6×18 cylinder, one of the sublattice staggered magnetizations becomes slightly negative because the central region no longer displays the expected perfect Néel staggered pattern, consistent with the strong suppression of Néel AFM order at this coupling. Previous studies have established a broad consensus that the PVBS phase terminates also at $J_1/J_2 \approx 0.78$ [17–21, 23–25,28]. So within the resolution of our calculations, we find no evidence for a stable intermediate QSL phase, supporting instead a direct transition between the PVBS and Néel AFM phases.

Conclusion

In this work, we investigate the lower boundary of the Néel AFM phase of the Shastry-Sutherland model using large-scale DMRG calculations. By employing staggered boundary pinning fields, we directly probe the bulk magnetic order parameter in the controversial region of $0.78 \leq J_1/J_2 \leq 0.81$. Our results demonstrate that the Néel AFM order remains finite at $J_1/J_2 = 0.8$, a point which was believed to lie in an intermediate spin liquid phase [18,19,24,28]. We find that the lower boundary of the Néel AFM phase lies near $J_1/J_2 \approx 0.78$, where the PVBS phase terminates [17–21,23–25,28]. These results provide evidence against an intermediate QSL phase in the Shastry-Sutherland model. Our findings instead support a direct transition between the PVBS and Néel AFM phases within the resolution of the present calculations. A related question concerns the nature of the phase transition: is it continuous, with a DQCP [17,22], or is it weakly first-order [21,25]? We believe that the present magnetization results in Fig. 1 cannot distinguish between these two scenarios. We leave this issue to future work, once accurate results for much larger system sizes become available.

Acknowledgments

The calculation in this work is carried out with TensorKit [47]. The computations in this paper were run on the Siyuan-1 cluster supported by the Center for High Performance Computing at Shanghai Jiao Tong University. MQ acknowledges the support from the National Natural Science Foundation of China (Grant Nos. 12522406 and 12274290), the Innovation Program for Quantum Science and Technology (Grant No. 2021ZD0301902), and the National Key Research and Development Program of MOST of China (Grant No. 2022YFA1405400).

References

[1] Anderson P W 1973 *Mater. Res. Bull.* **8** 153
[2] Anderson P W 1987 *Science* **235** 1196
[3] Balents L 2010 *Nature* **464** 199
[4] Savary L and Balents L 2016 *Rep. Prog. Phys.* **80** 016502
[5] Zhou Y, Kanoda K, and Ng T K 2017 *Rev. Mod. Phys.* **89** 025003
[6] Sriram Shastry B and Sutherland B 1981 *Physica B+C* **108** 1069
[7] Kageyama H, Yoshimura K, Stern R, Mushnikov N V, Onizuka K, Kato M, Kosuge K, Slichter C P, Goto T, and Ueda Y 1999 *Phys. Rev. Lett.* **82** 3168
[8] Koga A and Kawakami N 2000 *Phys. Rev. Lett.* **84** 4461
[9] Kodama K, Takigawa M, Horvatić M, Berthier C, Kageyama H, Ueda Y, Miyahara S, Becca F, and Mila F 2002 *Science* **298** 395
[10] Boos C, Crone S P G, Niesen I A, Corboz P, Schmidt K P, and Mila F 2019 *Phys. Rev. B* **100** 140413(R)
[11] Jiménez J L, Crone S P, Fogh E *et al*. 2021 *Nature* **592** 370
[12] Cui Y, Liu L, Lin H, Wu K H, Hong W, Liu X, Li C, Hu Z, Xi N, Li S, Yu R, Sandvik A W, and Yu W 2023 *Science* **380** 1179
[13] Cui Y, Du K, Wu Z, Li S, Yang P, Chen Y, Xu X, Chen H, Li C, Liu J, Wang B, Hong W, Li S, Xie Z, Cheng J, Normand B, Yu R, and Yu W 2025 arXiv:2411.00302 [cond-mat.str-el]
[14] Guo J, Wang P, Huang C *et al*. 2025 *Commun. Phys.* **8** 75
[15] Cui Y, Yu R, and Yu W 2025 *Chin. Phys. Lett.* **42** 047503
[16] Corboz P and Mila F 2013 *Phys. Rev. B* **87** 115144
[17] Lee J Y, You Y Z, Sachdev S, and Vishwanath A 2019 *Phys. Rev. X* **9** 041037
[18] Keleş A and Zhao E 2022 *Phys. Rev. B* **105** L041115
[19] Yang J, Sandvik A W, and Wang L 2022 *Phys. Rev. B* **105** L060409
[20] Wang L, Zhang Y, and Sandvik A W 2022 *Chin. Phys. Lett.* **39** 077502
[21] Xi N, Chen H, Xie Z Y, and Yu R 2023 *Phys. Rev. B* **107** L220408
[22] Liu W Y, Zhang X T, Wang Z, Gong S S, Chen W Q, and Gu Z C 2024 *Phys. Rev. Lett.* **133** 026502
[23] Chen H, Duan G, Liu C, Cui Y, Yu W, Xie Z Y, and Yu R 2025 arXiv: 2411.00301 [cond-mat.str-el]
[24] Viteritti L L, Rende R, Parola A, Goldt S, and Becca F 2025 *Phys. Rev. B* **111** 134411
[25] Qian X, Lv R, Lee J Y, and Qin M 2025 *Phys. Rev. B* **111** L241113
[26] Maity A, Ferrari F, Capponi S, Penc K, Potten J, Müller T, Feuerpfeil A, Thomale R, Lee J Y, Samajdar R, and Iqbal Y 2026 arXiv:2501.00096 [cond-mat.str-el]
[27] Chen L C and Liu Z X 2026 *Phys. Rev. B* **113** 224440
[28] Corboz P, Zhang Y, Ponsioen B, and Mila F 2026 *Phys. Rev. Lett.* **136** 186701
[29] Sandvik A W 2010 *AIP Conf. Proc.* **1297** 135
[30] Stoudenmire E and White S R 2012 *Annu. Rev. Condens. Matter Phys.* **3** 111
[31] Assaad F F and Herbut I F 2013 *Phys. Rev. X* **3** 031010
[32] White S R 1992 *Phys. Rev. Lett.* **69** 2863
[33] White S R 1993 *Phys. Rev. B* **48** 10345
[34] Schollwöck U 2011 *Ann. Phys.* **326** 96
[35] White S R and Chernyshev A L 2007 *Phys. Rev. Lett.* **99** 127004
[36] Östlund S and Rommer S 1995 *Phys. Rev. Lett.* **75** 3537
[37] Eisert J, Cramer M, and Plenio M B 2010 *Rev. Mod. Phys.* **82** 277
[38] Cirac J I, Pérez-García D, Schuch N, and Verstraete F 2021 *Rev. Mod. Phys.* **93** 045003
[39] Xiang T 2023 *Density Matrix and Tensor Network Renormalization* (Cambridge University Press)
[40] Gong S S, Zhu W, Sheng D N, Motrunich O I, and Fisher M P A 2014 *Phys. Rev. Lett.* **113** 027201
[41] Wang L and Sandvik A W 2018 *Phys. Rev. Lett.* **121** 107202
[42] Qian X and Qin M 2024 *Phys. Rev. B* **109** L161103
[43] Huang J, Qian X, and Qin M 2024 *J. Phys. Condens. Matter* **36** 185602
[44] Gallegos C A, Jiang S, White S R, and Chernyshev A L 2025 *Phys. Rev. Lett.* **134** 196702
[45] See Supplementary Materials for all truncation-error extrapolations of the staggered magnetization and bulk energies, as well as additional finite-size scaling results for the ground state energies at J_1/J_2 = 0.78, 0.79, and 0.81.
[46] Chen H, Fu Y, Yu W, Yu R, and Xie Z Y 2026 *Phys. Rev. B* **113** 155127
[47] Haegeman J The code is developed with TensorKit package at https://github.com/Jutho/TensorKit.jl